

Effect of the magnetic monopole charge on Dirac entanglement and Bell non-locality in Hayward spacetime

Abdessamie Chhieb^{1,2,*} and Mohamed Ouchrif^{1,2,†}

¹*Interdisciplinary Laboratory of Physics, Computer Science, and Oncology (LIPIO),
Mohamed First University, Oujda, Morocco*

²*National Institute For Particle Physics and Applications (NIPPA),
Oujda, Morocco*

We investigate the bipartite quantum correlations of Dirac fields in the background of a Hayward regular black hole, in which the central singularity is replaced by a de Sitter core characterised by the regularity parameter g . Two fermionic modes initially prepared in a Bell-type entangled state are shared between an asymptotic observer (Alice) and a static observer (Bob) hovering at fixed Schwarzschild-Hayward coordinate near the event horizon. Through the standard Damour–Ruffini single-mode Bogoliubov transformation, Bob’s mode splits into a physically accessible exterior mode B_I and a physically inaccessible interior mode B_{II} . We derive in closed form the reduced density matrices ρ_{AB_I} and $\rho_{AB_{II}}$ and quantify their quantum correlations through two complementary measures: the Wootters concurrence \mathcal{C} and the Clauser–Horne–Shimony–Holt (CHSH) Bell parameter \mathcal{B}_{\max} . We find that (i) the accessible correlations \mathcal{C}_I , \mathcal{B}_{\max}^I never vanish even in the infinite-temperature limit, the Pauli exclusion principle preventing total decoherence; (ii) the inaccessible correlations \mathcal{C}_{II} , \mathcal{B}_{\max}^{II} develop a non-zero value that witnesses the entanglement redistribution across the horizon, with \mathcal{C}_{II} approaching \mathcal{C}_I as $T_H \rightarrow \infty$; (iii) the accessible CHSH parameter violates the CHSH inequality at every finite, positive Hawking temperature for $\alpha = \pi/4$, with $\mathcal{B}_{\max}^I = 2\sqrt{2}/(\exp(-\omega/T_H) + 1)$, interpolating between the Tsirelson bound $2\sqrt{2}$ as $T_H \rightarrow 0$ and the classical limit 2 as $T_H \rightarrow \infty$; (iv) the inaccessible CHSH parameter is bounded above by the classical limit 2 and therefore never violates Bell’s inequality. The regularity parameter g enters all quantities only through the Hayward Hawking temperature, which decreases monotonically as g grows from 0 to the extremal value $g_c = (16/27)^{1/3}M \simeq 0.8399M$. A direct comparison with the bosonic (scalar-field) analogue, performed at matched values of the Hawking parameter, makes the fermionic origin of our results explicit: \mathcal{C}_I obeys the Pauli-protected lower bound $\sin(2\alpha)/\sqrt{2}$ and never vanishes, whereas the scalar concurrence decoheres completely in the infinite-temperature limit. The closed-form derivations suggest that singularity resolution and quantum-information preservation are connected through a single mechanism: the suppression of surface gravity at fixed ADM mass, mediated by Fermi–Dirac statistics.

I. INTRODUCTION

The black-hole information paradox [1, 2] remains one of the deepest open problems at the interface of quantum mechanics and gravity. A particularly fruitful avenue has been to study the fate of quantum entanglement of relativistic quantum fields propagating in black-hole backgrounds, since Hawking radiation degrades the quantum correlations measured by an exterior observer [3–10]. For Dirac fields in the Schwarzschild background, a body of work [7–10] has established that the Pauli exclusion principle prevents the complete loss of quantum correlations at infinite Hawking temperature, in sharp contrast with the bosonic case [11]. More recently, the analysis has been extended to charged Reissner–Nordström (RN) black holes [12], where the electric charge modulates the Hawking temperature and hence the rate of decoherence.

In this work, we extend the framework of relativistic quantum information to a *singularity-free* geometry, the Hayward regular black hole [13], whose central singularity is replaced by a de Sitter core regulated by a

length-scale parameter g . The motivation is threefold. First, regular black holes [13–17] are the simplest non-trivial generalisation of the Schwarzschild geometry that preserve the asymptotic structure while curing the curvature singularity; they thus provide a controlled laboratory in which to ask whether, and how, the absence of a singularity changes the quantum-information landscape near the horizon. Second, the Hayward temperature $T_H(g)$ is strictly smaller than the Schwarzschild temperature at fixed mass, and vanishes at the extremal value $g_c = (16/27)^{1/3}M \simeq 0.84M$, so a clean monotonic prediction can be made: as g increases, the rate of Hawking-induced decoherence *decreases*, and quantum correlations should be more efficiently preserved. Third, the recent characterisation of inner-horizon instabilities in regular black holes [18, 19] has identified the smoothing of the central singularity as a generic phenomenological feature of new physics at the horizon scale, which makes the quantum-information signatures of g a particularly clean probe.

We focus on two complementary quantifiers. (i) The Wootters concurrence [20] measures bipartite entanglement algebraically, with a simple closed form for X-states. (ii) The Clauser–Horne–Shimony–Holt (CHSH) Bell parameter [21, 22] probes nonlocal correlations

* Corresponding author: abdessamie.chhieb@ump.ac.ma

† m.ouchrif@ump.ac.ma

through the violation of the CHSH inequality. The two measures are complementary: a state can be entangled without violating any Bell inequality, so the joint analysis reveals which fraction of the entanglement survives as a Bell-nonlocal resource and which fraction is downgraded to a hidden-variable-compatible correlation. The combination of an algebraic quantifier (concurrence) and an inequality-based quantifier (CHSH) provides a sharper picture of decoherence than any single quantity alone.

Our analysis follows the single-mode Damour–Ruffini Bogoliubov convention [23, 24] adopted in the reference literature on Dirac fields in Schwarzschild [3, 6–9] and in the RN extension [12]. The validity and limitations of this approximation, in particular following the analyses of [25, 26].

The paper is organised as follows. Section II introduces the Hayward geometry and the associated Hawking temperature. Section III reviews the vacuum structure of the Dirac field. Section IV sets up the physical model, including a schematic representation of the setup in Fig. 1, and derives the reduced density matrices in both bipartitions. Sections V and VI compute the concurrence and the CHSH parameter, respectively, with explicit limits and Hayward dependence. Section VII presents the numerical results and discusses, figure by figure, the influence of the four control parameters (g, M, ω, α). Section IX summarises the main findings and indicates directions for future work. Throughout the paper we adopt natural units $G = \hbar = c = k_B = 1$.

II. HAYWARD BLACK HOLE GEOMETRY AND HAWKING TEMPERATURE

The line element of the Hayward regular black hole reads [13]

$$ds^2 = -f(r) dt^2 + f(r)^{-1} dr^2 + r^2 d\Omega^2, \quad (1)$$

with $d\Omega^2 = d\theta^2 + \sin^2\theta d\varphi^2$ and the lapse function

$$f(r) = 1 - \frac{2Mr^2}{r^3 + 2g^3}, \quad (2)$$

where M is the ADM mass and g the regularity (Hayward) parameter. For $g \rightarrow 0$ one recovers the Schwarzschild lapse $f(r) = 1 - 2M/r$. Near the origin, $f(r) \rightarrow 1 - Mr^2/g^3$, which is the de Sitter form with effective cosmological constant

$$\Lambda_{\text{eff}} = \frac{3M}{g^3}. \quad (3)$$

The Kretschmann scalar is finite everywhere, signalling the absence of any curvature singularity. The Hayward metric is sourced by a non-linear electrodynamics or by an effective stress-energy tensor representing quantum-gravity corrections [13, 16]; the exact origin of the source does not affect the propagation of probe Dirac fields on this background.

The event horizon r_+ is the largest real root of $f(r_+) = 0$,

$$r_+^3 - 2Mr_+^2 + 2g^3 = 0. \quad (4)$$

Real positive roots exist only for $g \leq g_c$. The extremal condition imposes Eq. (4) and its derivative $3r_+^2 - 4Mr_+ = 0$ to hold simultaneously, giving $r_+ = 4M/3$ and, after substitution,

$$g_c = \left(\frac{16}{27}\right)^{1/3} M \simeq 0.8399 M. \quad (5)$$

For $g > g_c$ no horizon exists and the metric describes a globally regular, horizonless object. Throughout this work we restrict the analysis to the physical regime $g \leq g_c$, where a regular black hole exists; we shall flag the unphysical extrapolation explicitly whenever a formula is evaluated outside this regime.

The Hawking temperature follows from the surface gravity $T_H = f'(r_+)/4\pi$. A direct computation of $f'(r)$ from Eq. (2) gives

$$f'(r) = \frac{2Mr(r^3 - 4g^3)}{(r^3 + 2g^3)^2}, \quad (6)$$

and hence

$$T_H = \frac{M r_+ (r_+^3 - 4g^3)}{2\pi (r_+^3 + 2g^3)^2}. \quad (7)$$

For $g = 0$, $r_+ = 2M$ and Eq. (7) reduces to the Schwarzschild result $T_H = 1/(8\pi M)$ [1]. The temperature vanishes at the extremal point $g = g_c$, where $r_+^3 = 4g_c^3$, signalling the absence of Hawking emission for an extremal Hayward black hole.

It is instructive to compare (7) with the analogous expression for the Bardeen regular black hole [14, 16], whose lapse function $f_{\text{Bar}}(r) = 1 - 2Mr^2/(r^2 + g^2)^{3/2}$ leads to

$$T_H^{\text{Bar}} = \frac{M r_+ (r_+^2 - 2g^2)}{2\pi (r_+^2 + g^2)^{5/2}}, \quad g_c^{\text{Bar}} = \frac{4M}{3\sqrt{3}} \simeq 0.7698 M. \quad (8)$$

Both geometries share the qualitative feature $T_H^{\text{RBH}}(g) < T_H^{\text{Schw}}$ at fixed M and r_+ , with extremality ($T_H \rightarrow 0$) reached at $g = g_c^{\text{RBH}}$. The Bardeen formula is provided here for completeness and will be referred to in Sec. VI when discussing the universal ordering of the CHSH parameter across regular geometries.

III. VACUUM STRUCTURE OF THE DIRAC FIELD

In a generic curved background, the Dirac equation reads [27]

$$[\gamma^a e_a^\mu (\partial_\mu + \Gamma_\mu)]\psi = 0, \quad (9)$$

with e_a^μ the inverse tetrad and Γ_μ the spin connection. In the Hayward metric, separating variables in the tortoise

coordinate $r_* = \int dr/f(r)$ leads, in the standard way [6, 24], to positive-frequency outgoing solutions outside and inside the event horizon:

$$\psi_k^{I+} = \zeta e^{-i\omega u}, \quad (r > r_+), \quad (10)$$

$$\psi_k^{II+} = \zeta e^{+i\omega u}, \quad (r < r_+), \quad (11)$$

where ζ is a four-component Dirac spinor and $u = t - r_*$ the retarded null coordinate. Following the Damour–Ruffini analytic continuation [23] and the single-mode Bogoliubov treatment used throughout the Dirac relativistic-quantum-information literature [3, 6–9, 12], the Kruskal vacuum and the single-particle excited state of mode k are related to the corresponding Schwarzschild–Hayward Fock states by

$$|0\rangle_K = \frac{|0\rangle_I \otimes |0\rangle_{II}}{\sqrt{e^{-\omega/T_H} + 1}} + \frac{|1\rangle_I \otimes |1\rangle_{II}}{\sqrt{e^{\omega/T_H} + 1}}, \quad (12)$$

$$|1\rangle_K = |1\rangle_I \otimes |0\rangle_{II}. \quad (13)$$

Here, the state $|n\rangle_I$ ($|n\rangle_{II}$) is the n -particle excitation of the outgoing mode in region I (II). The vacuum (12) is the unique vacuum seen by a static observer hovering at fixed coordinate $r = r_+ + \epsilon$ outside the horizon, in the Boulware–Hartle–Hawking sense [28–30]; we elaborate on this in Sec. VIII.

The Pauli exclusion principle restricts Eq. (12) to only two terms, in contrast with the infinite geometric sum that arises for bosonic fields [11, 31]. Explicitly, for a scalar (spin-0) field the Bogoliubov transformation produces an infinite-dimensional Fock decomposition,

$$|0\rangle_K^{\text{bos}} = \frac{1}{\cosh r_\omega} \sum_{n=0}^{\infty} (\tanh r_\omega)^n |n\rangle_I |n\rangle_{II}, \quad (14)$$

whereas Pauli exclusion truncates the Dirac sector to the two-level decomposition of Eq. (12) [32, 33]. This truncation is physically significant: it bounds the entanglement entropy and modifies the concurrence structure, so that the maximal entanglement degradation for fermionic modes remains *bounded*, whereas bosonic modes can undergo complete decoherence in the infinite-temperature limit. Equivalently, the anticommutation relations of the fermionic field operators impose the unitarity constraint $|\alpha_\omega|^2 + |\beta_\omega|^2 = 1$ on the Bogoliubov coefficients, in contrast with the bosonic relation $|\alpha_\omega|^2 - |\beta_\omega|^2 = 1$ [34]; this constraint is responsible for the X-type form of the reduced density matrices ϱ_{AB_I} and $\varrho_{AB_{II}}$ derived below, and has no bosonic analogue. The thermal occupation that the exterior observer ultimately reads off therefore carries a *Fermi–Dirac* factor $(e^{\omega/T_H} + 1)^{-1}$, whereas the bosonic counterpart would be the *Bose–Einstein* factor $(e^{\omega/T_H} - 1)^{-1}$ that diverges as $T_H \rightarrow \infty$. The structural lower bound on the accessible concurrence reported in Eq. (26) below is a direct consequence of this difference.

We introduce the convenient abbreviations

$$p \equiv \frac{1}{e^{-\omega/T_H} + 1}, \quad q \equiv \frac{1}{e^{\omega/T_H} + 1}, \quad p + q = 1, \quad (15)$$

so that Eq. (12) takes the compact form

$$|0\rangle_K = \sqrt{p} |0\rangle_I |0\rangle_{II} + \sqrt{q} |1\rangle_I |1\rangle_{II}. \quad (16)$$

The Hayward specificity enters only through $T_H = T_H(g, M, r_+)$ via Eq. (7).

IV. PHYSICAL MODEL AND REDUCED DENSITY MATRICES

A. Setup

We consider two fermionic modes A and B initially prepared in a Bell-type entangled state

$$|\psi\rangle_{AB} = \cos \alpha |0\rangle_A |0\rangle_B + \sin \alpha |1\rangle_A |1\rangle_B, \quad (17)$$

where $\alpha \in [0, \pi/2]$ controls the initial entanglement; $\alpha = 0, \pi/2$ correspond to product states and $\alpha = \pi/4$ to the maximally entangled Bell state. For brevity we write $a \equiv \cos \alpha$, $b \equiv \sin \alpha$. Alice carries mode A and remains in the asymptotically flat region; Bob carries mode B and is a *static observer* at fixed coordinate $r = r_+ + \epsilon$ outside the event horizon, so that his accelerated worldline samples the Hartle–Hawking vacuum. (A free-falling observer would see no Hawking quanta in the equivalent-principle sense; the splitting (12) pertains to the static observer.) The Hawking effect splits Bob’s Kruskal mode into an exterior (accessible) component B_I and an interior (inaccessible) component B_{II} , as depicted in Fig. 1.

B. Tripartite state in Hayward modes

Substituting Eqs. (13) and (16) into (17), with Alice’s mode untouched, we expand $|0\rangle_B \rightarrow \sqrt{p} |0\rangle_{B_I} |0\rangle_{B_{II}} + \sqrt{q} |1\rangle_{B_I} |1\rangle_{B_{II}}$ and $|1\rangle_B \rightarrow |1\rangle_{B_I} |0\rangle_{B_{II}}$. The initial state becomes the tripartite pure state

$$|\psi\rangle_{AB_I B_{II}} = a\sqrt{p} |000\rangle + a\sqrt{q} |011\rangle + b |110\rangle. \quad (18)$$

Normalisation is preserved: $a^2 p + a^2 q + b^2 = a^2 + b^2 = 1$.

C. Reduced state ϱ_{AB_I} (accessible)

Since B_{II} is causally hidden behind r_+ for the static external observer, we must trace it out. A term $|\phi_i\rangle\langle\phi_j|$ of $|\psi\rangle\langle\psi|$ survives the partial trace over B_{II} if and only if the two B_{II} labels coincide. Of the nine cross-terms of (18), five survive: the three diagonal terms plus the two cross-terms between $|000\rangle$ and $|110\rangle$, since both have $B_{II} = 0$. Collecting them in the computational basis $\{|00\rangle, |01\rangle, |10\rangle, |11\rangle\}$ for (A, B_I) ,

$$\varrho_{AB_I} = \begin{pmatrix} a^2 p & 0 & 0 & ab\sqrt{p} \\ 0 & a^2 q & 0 & 0 \\ 0 & 0 & 0 & 0 \\ ab\sqrt{p} & 0 & 0 & b^2 \end{pmatrix}. \quad (19)$$

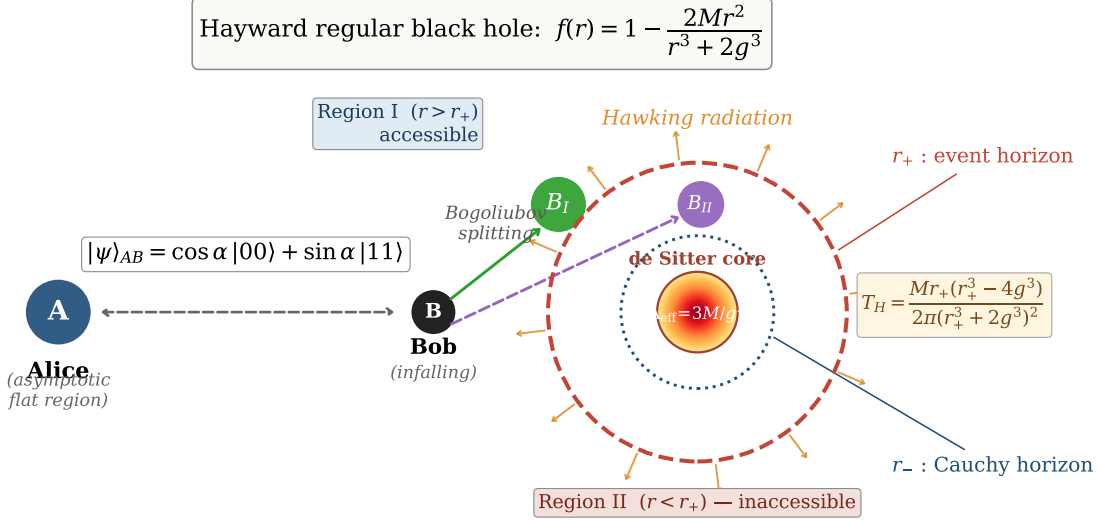


FIG. 1: Schematic representation of the physical setup. Alice, with qubit A , stays in the asymptotically flat region. Bob, with qubit B , hovers statically at fixed Schwarzschild–Hayward coordinate $r = r_+ + \epsilon$ near the event horizon of a Hayward regular black hole whose central singularity is replaced by a de Sitter core (orange) of effective cosmological constant $\Lambda_{\text{eff}} = 3M/g^3$. The metric admits an inner Cauchy horizon r_- (blue dotted) and an event horizon r_+ (red dashed). At r_+ , Bob’s mode splits via the Damour–Ruffini Bogoliubov transformation into an exterior mode B_I (accessible) and an interior mode B_{II} (causally hidden behind r_+). Hawking radiation, sourced by the surface gravity at r_+ with temperature T_H , decoheres the initial Bell state $|\psi\rangle_{AB}$.

This is an X-type density matrix. Trace and positivity are immediate: $\text{tr } \varrho_{AB_I} = a^2(p + q) + b^2 = 1$, and the spectrum is $\{a^2p + b^2, a^2q, 0, 0\} \succeq 0$.

D. Reduced state $\varrho_{AB_{II}}$ (inaccessible)

An analogous calculation, this time tracing over B_I , retains the diagonal terms plus the cross-terms between $|011\rangle$ and $|110\rangle$ (both have $B_I = 1$). The result reads

$$\varrho_{AB_{II}} = \begin{pmatrix} a^2p & 0 & 0 & 0 \\ 0 & a^2q & ab\sqrt{q} & 0 \\ 0 & ab\sqrt{q} & b^2 & 0 \\ 0 & 0 & 0 & 0 \end{pmatrix}. \quad (20)$$

The spectrum is $\{a^2p, a^2q + b^2, 0, 0\}$. Both Eqs. (19) and (20) are X-shaped in the computational basis, which dramatically simplifies the evaluation of all three quantum-information measures used below.

V. WOOTTERS CONCURRENCE

For an arbitrary two-qubit state ϱ , the Wootters concurrence [20] is

$$C(\varrho) = \max\{0, \sqrt{\lambda_1} - \sqrt{\lambda_2} - \sqrt{\lambda_3} - \sqrt{\lambda_4}\}, \quad (21)$$

with λ_i the eigenvalues, in decreasing order, of $R = \varrho(\sigma_y \otimes \sigma_y) \varrho^*(\sigma_y \otimes \sigma_y)$. For an X-state with elements ϱ_{ij} , Eq. (21) reduces to [35]

$$C(\varrho_X) = 2 \max\{0, |\varrho_{14}| - \sqrt{\varrho_{22}\varrho_{33}}, |\varrho_{23}| - \sqrt{\varrho_{11}\varrho_{44}}\}. \quad (22)$$

From Eq. (19): $\varrho_{14} = ab\sqrt{p}$, $\varrho_{23} = 0$, $\varrho_{22}\varrho_{33} = 0$, and $\varrho_{11}\varrho_{44} = a^2b^2p$, whence

$$\mathcal{C}_I = C(\varrho_{AB_I}) = 2ab\sqrt{p} = \frac{\sin 2\alpha}{\sqrt{e^{-\omega/T_H} + 1}}. \quad (23)$$

Similarly, from Eq. (20): $\varrho_{14} = 0$, $\varrho_{23} = ab\sqrt{q}$, $\varrho_{11}\varrho_{44} = 0$, $\varrho_{22}\varrho_{33} = a^2b^2q$, so

$$\mathcal{C}_{II} = C(\varrho_{AB_{II}}) = 2ab\sqrt{q} = \frac{\sin 2\alpha}{\sqrt{e^{\omega/T_H} + 1}}. \quad (24)$$

Limits. As $T_H \rightarrow 0$: $p \rightarrow 1$, $q \rightarrow 0$, $\mathcal{C}_I \rightarrow \sin 2\alpha$ (initial Bell entanglement preserved in the accessible sector), $\mathcal{C}_{II} \rightarrow 0$ (no entanglement leaks to the interior). As $T_H \rightarrow \infty$: $p, q \rightarrow 1/2$, both \mathcal{C}_I and \mathcal{C}_{II} tend to $\sin(2\alpha)/\sqrt{2} > 0$, a fermionic protection against total entanglement loss due to Pauli exclusion [7, 9, 12], witnessing the symmetric redistribution of entanglement between the two sectors. This is in sharp contrast with scalar (bosonic) fields, for which the infinite geometric sum in the Bogoliubov decomposition leads to $\mathcal{C}_I \rightarrow 0$

as $T_H \rightarrow \infty$ [11, 12], i.e. complete decoherence. The Pauli exclusion principle thus provides a structural lower bound $\mathcal{C}_I \geq \sin(2\alpha)/\sqrt{2}$ that has no bosonic analogue.

Hayward dependence. Both (23) and (24) depend on g only through $T_H = T_H(g, M, r_+)$. Since T_H decreases monotonically with g in the physical regime $g \leq g_c$,

$$\frac{\partial \mathcal{C}_I}{\partial g} \geq 0, \quad \frac{\partial \mathcal{C}_{II}}{\partial g} \leq 0, \quad (25)$$

at fixed M and ω . The regularity parameter therefore enhances the entanglement in the exterior and suppresses that leaking to the interior; at extremality $g = g_c$, the initial Bell state is fully preserved ($\mathcal{C}_I = \sin 2\alpha$, $\mathcal{C}_{II} = 0$).

Analytic structure and non-monotonic behaviour. The Hayward Hawking temperature $T_H(g, M, r_+)$ of Eq. (7) vanishes at the extremal locus $r_+ = 4^{1/3}g$ and as $r_+ \rightarrow \infty$, and reaches an interior maximum $T_H^{\max} = T_H^{\max}(g, M)$ at an intermediate radius $r_+^* = r_+^*(g, M)$ controlled by the mass-regularity ratio. Because $\mathcal{C}_I = \sin(2\alpha)/\sqrt{1 + e^{-\omega/T_H}}$ is a monotonically *decreasing* function of T_H at fixed ω and α , the concurrence inherits a non-monotonic dependence on r_+ :

- at $r_+ = 4^{1/3}g$ (extremal limit): $T_H = 0$, $e^{-\omega/T_H} \rightarrow 0$, and $\mathcal{C}_I \rightarrow \sin(2\alpha)$ (maximal preservation);
- at $r_+ = r_+^*(g, M)$ (maximum temperature): \mathcal{C}_I reaches its minimum, corresponding to the strongest Hawking effect;
- as $r_+ \rightarrow \infty$: $T_H \rightarrow 0$ again, and \mathcal{C}_I recovers towards $\sin(2\alpha)$.

This non-monotonic behaviour, sharply visible in Figs. 2–3 below, has no analogue in the Schwarzschild case ($g = 0$), where $T_H = 1/(4\pi r_+)$ is monotonically decreasing and \mathcal{C}_I monotonically increases with r_+ [36]. The Hayward regularity scale therefore introduces a qualitatively new feature in the entanglement landscape, parallel to that observed in the Reissner–Nordström [12] and dilatonic [10] contexts but with the characteristic Hayward signature $r_+^{\text{(ext)}} = 4^{1/3}g \simeq 1.587g$.

The transition thresholds at which \mathcal{C}_I drops below a chosen level ε follow analytically from $T_H(r_+^\dagger, g, M) = \omega/\ln(1/\varepsilon^2 - 1)^{-1}$, giving $r_+^\dagger \simeq 4^{1/3}g(1 + \delta_\omega)$ with a small, ω -dependent correction δ_ω that scales linearly with g . This linear scaling underlies the regular spacing of the charge-induced transitions of Fig. 2, in agreement with the numerical curves.

Frequency limits. In the high-frequency limit $\omega \rightarrow \infty$ one has $p \rightarrow 1$ and $q \rightarrow 0$, yielding $\mathcal{C}_I \rightarrow \sin(2\alpha)$ (maximal preservation) and $\mathcal{C}_{II} \rightarrow 0$. Conversely, in the low-frequency limit $\omega \rightarrow 0$ at fixed $T_H > 0$, both p and q tend to $1/2$, leading to the symmetric plateau $\mathcal{C}_I = \mathcal{C}_{II} = \sin(2\alpha)/\sqrt{2}$. These two analytical limits explain quantitatively both the low-frequency plateau and the high-frequency enhancement that will be seen in Fig. 4 below, in line with the dilatonic [37] and the RN [12] analyses.

Fermionic lower bound. The plateau value $\sin(2\alpha)/\sqrt{2}$ is the universal lower bound of the accessible fermionic concurrence in the present setting:

$$\mathcal{C}_I \geq \frac{\sin 2\alpha}{\sqrt{2}} \quad (\text{for any } T_H > 0). \quad (26)$$

This bound is a direct consequence of the Fermi–Dirac statistics discussed below Eq. (14): the +1 in the denominator of $\mathcal{C}_I = \sin(2\alpha)/\sqrt{1 + e^{-\omega/T_H}}$ enforces a maximum of 2 in the Fermi–Dirac factor, whereas the analogous Bose–Einstein factor $(e^{\omega/T_H} - 1)^{-1}$ diverges as $T_H \rightarrow \infty$ and can lead to complete decoherence. The fermionic concurrence therefore never vanishes completely regardless of the values of g , ω , or r_+ in the physical Hayward range, a feature that we will visualise in Fig. 6 through a direct comparison with the scalar-field analogue.

VI. BELL–CHSH NON-LOCALITY

The CHSH operator [21, 22] is

$$\mathcal{B}_{\text{CHSH}} = \mathbf{a} \cdot \boldsymbol{\sigma} \otimes (\mathbf{b} + \mathbf{b}') \cdot \boldsymbol{\sigma} + \mathbf{a}' \cdot \boldsymbol{\sigma} \otimes (\mathbf{b} - \mathbf{b}') \cdot \boldsymbol{\sigma}, \quad (27)$$

with $\mathbf{a}, \mathbf{a}', \mathbf{b}, \mathbf{b}'$ unit vectors of \mathbb{R}^3 , and the CHSH inequality is $|\langle \mathcal{B}_{\text{CHSH}} \rangle| \leq 2$. The Tsirelson bound [38] sets the quantum maximum at $2\sqrt{2}$. For a generic two-qubit state ϱ , the Horodecki criterion gives

$$\mathcal{B}_{\max}(\varrho) = 2\sqrt{M(\varrho)}, \quad M(\varrho) = t_i^2 + t_j^2, \quad (28)$$

where t_i^2, t_j^2 are the two largest of $T_{11}^2, T_{22}^2, T_{33}^2$, and $T_{ii} = \text{tr}[\varrho \sigma_i \otimes \sigma_i]$ are the diagonal components of the correlation tensor. For an X-state with real off-diagonals,

$$\begin{aligned} T_{11} &= 2(\varrho_{14} + \varrho_{23}), \\ T_{22} &= 2(\varrho_{23} - \varrho_{14}), \\ T_{33} &= \varrho_{11} - \varrho_{22} - \varrho_{33} + \varrho_{44}. \end{aligned} \quad (29)$$

A. Accessible CHSH parameter

From Eq. (19): $T_{11}^I = -T_{22}^I = \sin 2\alpha \sqrt{p}$, $T_{33}^I = 1 - 2\alpha^2 q$. For $\alpha = \pi/4$, $(T_{11}^I)^2 = (T_{22}^I)^2 = p$, $(T_{33}^I)^2 = p^2 \leq p$, so the two largest squared components are $\{p, p\}$ and

$$\mathcal{B}_{\max}^I|_{\alpha=\pi/4} = 2\sqrt{2p} = \frac{2\sqrt{2}}{\sqrt{e^{-\omega/T_H} + 1}}. \quad (30)$$

Limits and Bell violation. (i) $T_H \rightarrow 0$: $p \rightarrow 1$, $\mathcal{B}_{\max}^I \rightarrow 2\sqrt{2}$, the Tsirelson bound. (ii) $T_H \rightarrow \infty$: $p \rightarrow 1/2$, $\mathcal{B}_{\max}^I \rightarrow 2$, the classical limit. (iii) Bell violation requires $\mathcal{B}_{\max}^I > 2$, i.e. $p > 1/2$, which holds if and only if $T_H > 0$ (since $e^{-\omega/T_H} < 1$ for any finite positive ω and T_H). Consequently, the accessible state at

$\alpha = \pi/4$ violates the CHSH inequality at every finite, strictly positive Hawking temperature, i.e. for all Hayward black holes with $g < g_c$.

For arbitrary α ,

$$M(\varrho_{AB_1}) = p \sin^2 2\alpha + \max\{p \sin^2 2\alpha, (1 - 2a^2 q)^2\}. \quad (31)$$

B. Inaccessible CHSH parameter

From Eq. (20): $T_{11}^{\text{II}} = T_{22}^{\text{II}} = \sin 2\alpha \sqrt{q}$, $T_{33}^{\text{II}} = 2a^2 p - 1$. At $\alpha = \pi/4$, $a^2 = 1/2$, $T_{33}^{\text{II}} = p - 1 = -q$, so

$$\mathcal{B}_{\text{max}}^{\text{II}}|_{\alpha=\pi/4} = 2\sqrt{2q} = \frac{2\sqrt{2}}{\sqrt{e^{\omega/T_H} + 1}} \leq 2. \quad (32)$$

Violation would require $q > 1/2$, impossible since $q \in (0, 1/2)$. The inaccessible state never violates CHSH, in agreement with the corresponding results for Schwarzschild [7, 9] and RN [12].

C. Universal ordering at fixed M

As shown in Sec. II, both the Hayward and Bardeen geometries have $T_H^{\text{RBH}} \leq T_H^{\text{Schw}}$ at fixed M and r_+ , with extremality reached at $g_c^{\text{Hay}} \simeq 0.840 M$ and $g_c^{\text{Bar}} \simeq 0.770 M$. The CHSH parameter being a monotonically *decreasing* function of T_H in the accessible sector, this implies

$$\mathcal{B}_{\text{max}}^{\text{I}}|_{\text{Schw}} \leq \mathcal{B}_{\text{max}}^{\text{I}}|_{\text{Bar}} \leq \mathcal{B}_{\text{max}}^{\text{I}}|_{\text{Hay}} \quad \text{at fixed } M, r_+, \omega. \quad (33)$$

This ordering, which is a strict mathematical consequence of the explicit forms (7)–(8) and of the Pauli-protected single-mode structure, formalises the qualitative statement that *regular geometries preserve quantum non-locality more efficiently than their singular Schwarzschild counterpart at fixed ADM mass*. We stress that the comparison is performed at a common value of the Schwarzschild radial coordinate r_+ ; for each geometry, r_+ is related to M and g through the respective horizon equation, so the physical interpretation of r_+ as an areal radius is shared, but the internal structure of the geometry (de Sitter core versus singularity) differs.

VII. NUMERICAL RESULTS AND DISCUSSION

Before turning to the full parameter scans, we collect in Table I the analytical limiting values of all six bipartite measures at $\alpha = \pi/4$, for the two extreme regimes $T_H \rightarrow 0$ (cold, extremal Hayward limit or large r_+) and $T_H \rightarrow \infty$ (hot, small r_+ Schwarzschild limit). These benchmarks provide a useful reference for the figures that follow.

TABLE I: Limiting values of the bipartite measures at $\alpha = \pi/4$. $p \rightarrow 1$, $q \rightarrow 0$ as $T_H \rightarrow 0$; $p, q \rightarrow 1/2$ as $T_H \rightarrow \infty$.

Quantity	$T_H \rightarrow 0$	$T_H \rightarrow \infty$
\mathcal{C}_{I}	1	$1/\sqrt{2} \simeq 0.707$
\mathcal{C}_{II}	0	$1/\sqrt{2} \simeq 0.707$
$\mathcal{B}_{\text{max}}^{\text{I}}$	$2\sqrt{2} \simeq 2.828$	2
$\mathcal{B}_{\text{max}}^{\text{II}}$	0	2

We now report a systematic numerical exploration of $\mathcal{C}_{\text{I}}, \mathcal{C}_{\text{II}}, \mathcal{B}_{\text{max}}^{\text{I}}, \mathcal{B}_{\text{max}}^{\text{II}}$ as functions of the event-horizon radius r_+ , scanning in turn the Hayward parameter g , the mass M , the mode frequency ω , and the initial entanglement angle α . Throughout, we treat r_+ as the natural control parameter, recalling that the Hayward black-hole regime requires $r_+^3 \geq 4g^3$, equivalently $r_+ \geq 4^{1/3}g \simeq 1.587g$, so that the surface gravity at r_+ (and hence T_H) is non-negative. For $r_+ < 4^{1/3}g$ the formulae (23)–(32) can still be evaluated formally but correspond to an unphysical extrapolation; this region is shaded in grey in the figures, and the curves with $g > 0$ are drawn only in their physical domain. The frequency is fixed at $\omega M = 0.05$, comparable to the Schwarzschild temperature scale $T_H^{\text{Schw}} M = 1/(8\pi) \simeq 0.04$, so that the Hawking-induced decoherence is clearly visible in the plotting range $r_+/M \in [0, 6]$.

Figure 2 contrasts the Schwarzschild reference ($g = 0$) with three increasing physical values of the Hayward parameter, $g/M \in \{0.30, 0.60, 0.83\}$, at fixed mass $M = 1$ and Bell-state initialisation $\alpha = \pi/4$. (We emphasise that all four values are below $g_c/M \simeq 0.84$; the formulas are evaluated in the physical black-hole regime throughout.) The qualitative response is dictated by the monotonic decrease of T_H with g , but the individual panels reveal a richer structure that we now dissect.

a. Accessible concurrence \mathcal{C}_{I} (panel a). The Schwarzschild curve (solid blue) starts at $\mathcal{C}_{\text{I}} \simeq 0.71$ as $r_+ \rightarrow 0^+$, exactly the Pauli-protected residual value $\sin(\pi/4)\sqrt{p}|_{p=1/2} = 1/\sqrt{2}$ that one would obtain in the $T_H \rightarrow \infty$ limit. As r_+ grows, the Schwarzschild $T_H = 1/(8\pi r_+)$ decreases, $p \rightarrow 1$, and $\mathcal{C}_{\text{I}} \rightarrow \sin(2 \cdot \pi/4) = 1$, i.e. the full Bell entanglement is recovered for a sufficiently large (cold) hole. The Hayward curves with $g > 0$ exhibit a sharp threshold behaviour: below the extremal locus $r_+^{(\text{ext})} = 4^{1/3}g$, the surface gravity is negative and the formal extrapolation of (23) returns small or zero values; above the threshold, the physical near-extremal Hawking temperature is so small that \mathcal{C}_{I} quickly approaches unity. The threshold shifts to larger r_+ as g grows: $r_+^{(\text{ext})}/M \simeq 0.476, 0.953, 1.318$ for $g/M = 0.30, 0.60, 0.83$ respectively, in exact agreement with the analytic formula $r_+^3 = 4g^3$. The three Hayward curves saturate $\mathcal{C}_{\text{I}} = 1$ within a window of width $\Delta r_+/M \lesssim 0.3$ above their respective thresholds,

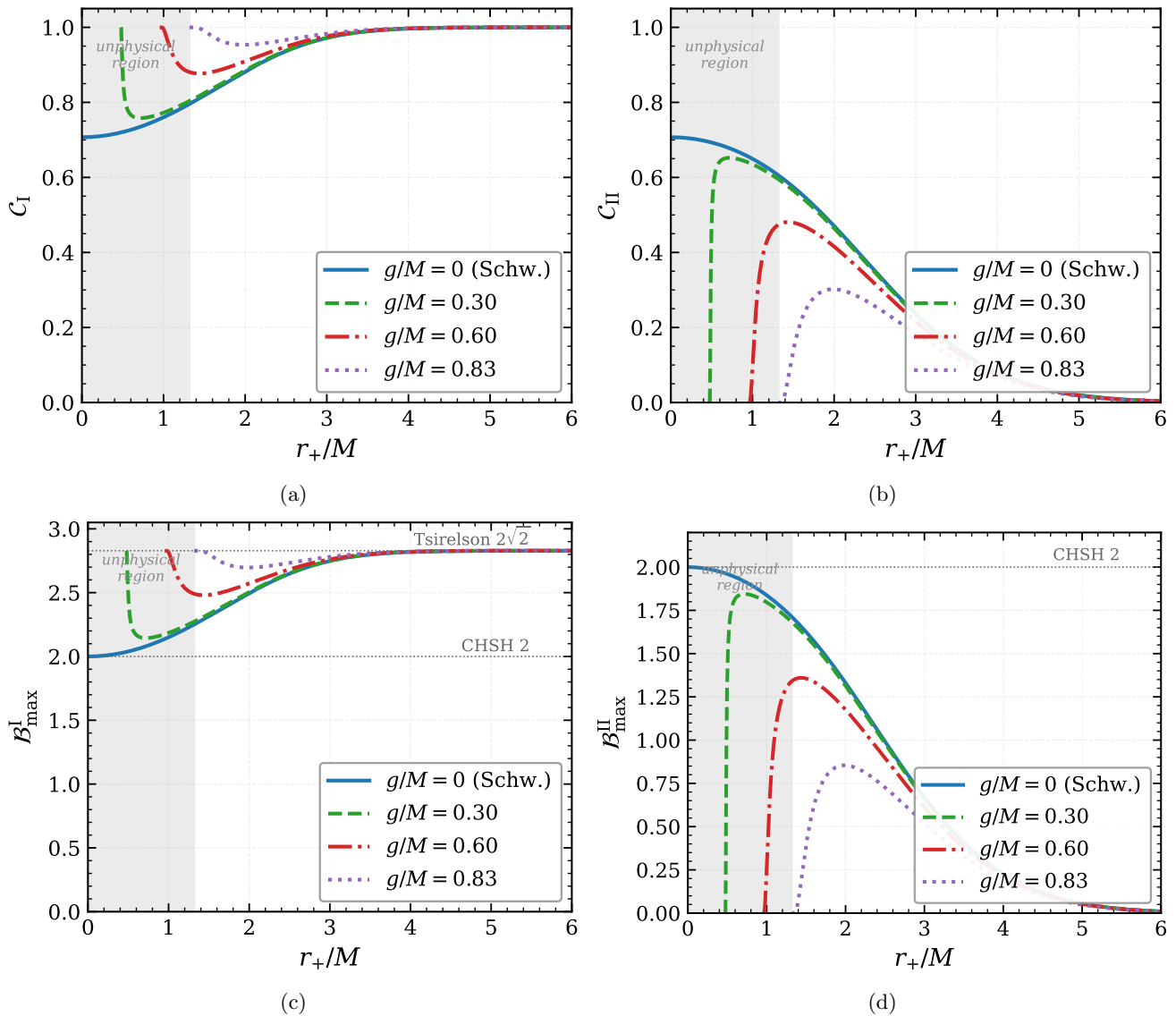


FIG. 2: Concurrences C_I, C_{II} (panels a,b) and CHSH parameters $\mathcal{B}_{\max}^I, \mathcal{B}_{\max}^{II}$ (panels c,d) as functions of r_+/M , for four *physical* values of the Hayward parameter $g/M \in \{0, 0.30, 0.60, 0.83\}$, all in the regime $g \leq g_c \simeq 0.84 M$ where the Hayward solution describes a regular black hole. Parameters: $M = 1, \omega = 0.05, \alpha = \pi/4$. Horizontal dotted lines mark the Tsirelson bound $2\sqrt{2}$ and the classical CHSH limit 2. The light grey band indicates the unphysical region $r_+ < 4^{1/3}g_{\max}$, where no event horizon exists for the largest g value; curves with $g > 0$ are drawn only in their respective physical domains $r_+ > 4^{1/3}g$.

demonstrating that the Hayward regularity efficiently cools the black hole, so that even a near-extremal Hayward horizon already produces an accessible Bell state with C_I within a few percent of unity.

b. Inaccessible concurrence C_{II} (panel b). The mirror behaviour in panel (b) is equally instructive. The Schwarzschild curve starts at $C_{II} \simeq 0.71$ (the same Pauli-protected redistribution maximum) and decreases monotonically, more rapidly than the saturation in panel (a) because $C_{II} \propto \sqrt{q}$ involves the smaller of the two Bogoliubov weights. By $r_+/M = 2$ the Schwarzschild C_{II} has already dropped below 0.15. The Hayward curves

with $g/M \geq 0.30$ are essentially zero throughout the physical regime $r_+ \geq 4^{1/3}g$ above the threshold, with a small bump localised near it. The combination of panels (a) and (b) makes it manifest that, in the Hayward setting, the redistribution effect [7, 8] so prominent in Schwarzschild is essentially shut off.

c. Accessible CHSH parameter \mathcal{B}_{\max}^I (panel c). The two horizontal dotted reference lines mark the classical Bell limit ($\mathcal{B}_{\max}^I = 2$) and the Tsirelson bound ($\mathcal{B}_{\max}^I = 2\sqrt{2}$). For Schwarzschild, \mathcal{B}_{\max}^I rises smoothly from 2 at $r_+ \rightarrow 0^+$ to $2\sqrt{2}$ as $r_+ \rightarrow \infty$; Bell non-locality is present at every finite r_+ , but the strength of the vi-

olation is graded by the horizon radius. The Hayward curves trade the smooth Schwarzschild interpolation for a sharper transition: above the threshold the cold near-extremal T_H is so small that \mathcal{B}_{\max}^I reaches $2\sqrt{2}$ within a narrow window. The two regimes are therefore physically distinct: in Schwarzschild one trades horizon radius for Bell violation strength, while in Hayward (any $g > 0$) one obtains near-maximal quantum violation throughout the physical regime above the threshold.

d. Inaccessible CHSH parameter $\mathcal{B}_{\max}^{\text{II}}$ (panel d). Panel (d) confirms the no-go bound $\mathcal{B}_{\max}^{\text{II}} \leq 2$ throughout the physical regime regardless of g , since $q \leq 1/2$ identically. The Schwarzschild curve attains $\mathcal{B}_{\max}^{\text{II}} = 2$ (the classical limit) only in the infinite-temperature limit $r_+ \rightarrow 0^+$ and decreases monotonically with r_+ . For $g/M \geq 0.30$ the curve is essentially zero everywhere in the physical regime. The two key lessons from Fig. 2 are: (i) the Hayward regularity enhances the survival of Bell non-locality in the accessible sector relative to Schwarzschild; (ii) the inaccessible Bell parameter is rigorously capped at the classical limit, a no-go robust against the regularity correction.

Figure 3 fixes $g/M = 0.5$ (always inside the physical window $g \leq g_c$) and scans the black-hole mass $M \in \{0.5, 1, 2, 5\}$. The role of M is most simply understood in the Schwarzschild limit, where $T_H^{\text{Schw}} = 1/(8\pi M)$: heavier holes are colder, and the rate of Hawking-induced decoherence drops accordingly. The Hayward formula (7) preserves this monotonic trend: at fixed r_+ , larger M leads to smaller T_H and hence larger p and smaller q . The four mass curves all transit through the threshold $r_+^{\text{(ext)}}/M = 4^{1/3} \cdot 0.5 \simeq 0.79$, which is the same in units of M . The visible difference among the curves at fixed r_+/M reflects the explicit M -dependence of T_H , which is non-trivially inherited through the cubic horizon equation (4).

e. Connection to relativistic quantum metrology. At fixed regularity ratio g/M , the visible spread of curves in Fig. 3 translates into a sensitivity of the bipartite measures to the absolute mass scale. From the perspective of relativistic quantum information [39–41], this sensitivity may be exploited as a quantum-thermometric probe of the near-horizon geometry, with the X-state closed form (19)–(20) allowing for a fully analytical computation of the quantum Fisher information.

The robustness to changes of mode frequency is investigated in Fig. 4, at fixed $M = 1$, $g = 0.5$, $\alpha = \pi/4$, for $\omega M \in \{0.02, 0.05, 0.10, 0.30\}$. The fundamental dimensionless parameter controlling the Hawking factor is ω/T_H : as ω grows, $e^{-\omega/T_H}$ becomes exponentially small for any positive T_H , $p \rightarrow 1$, and the reduced state ρ_{AB_1} approaches the initial Bell state. The figure shows that the saturation threshold shifts to smaller r_+ as ω increases, in agreement with the $\omega^{-1/2}$ scaling of the half-saturation point predicted by the Schwarzschild small- g analysis. The inaccessible quantities are correspondingly suppressed: for $\omega M = 0.30$ the curves are essentially zero everywhere in the physical regime, while for $\omega M = 0.02$

a sizeable bump persists above the threshold. From the relativistic-quantum-information perspective [39–41], encoding logical qubits on high-energy modes minimises the gravitational degradation of the quantum-information resource. The novelty in the Hayward setting is that the threshold for saturation is reached at smaller r_+ than in Schwarzschild, owing to the smaller T_H , an additional layer of robustness conferred by the regularity.

Figure 5 explores how the initial mixing angle α conditions the survival of quantum correlations. The closed-form expressions (23)–(24) and (31) cleanly separate the α -dependence from the geometric content: the concurrences scale as $|\sin 2\alpha|$, which makes the Bell angle $\alpha = \pi/4$ uniquely optimal. The CHSH parameter has a more involved α -dependence inherited from the competition between the $\sin 2\alpha$ -controlled T_{11}, T_{22} components and the α -dependent T_{33} component. As a quantitative example, for $\alpha = \pi/8$ and $p \simeq 1$ a direct evaluation of (31) gives $M(\rho_{AB_1}) \simeq 3/2$, hence $\mathcal{B}_{\max}^I \simeq \sqrt{6} \simeq 2.449$, which is just visible in panel (c) as the upper plateau of the $\alpha = \pi/8$ curve. A practical implication is that small preparation errors $|\delta\alpha| \ll 1$ around $\alpha = \pi/4$ cost only $\mathcal{O}(\delta\alpha^2)$ in the Bell violation strength, providing a useful robustness margin for experimental implementations.

To make the fermionic character of our results fully explicit, we conclude the parameter survey with Fig. 6, in which the Dirac (spin-1/2) concurrence is compared directly with the analogous scalar (spin-0) concurrence at matched values of the Hawking parameter $\sin^2 r_\omega$. As emphasised at Eq. (14), the Pauli exclusion principle truncates the fermionic Fock space to two levels per mode, which translates analytically into the lower bound (26). The bosonic concurrence, by contrast, is unconstrained from below and crosses zero in the infinite-temperature limit, corresponding to complete decoherence. Panels (a)–(d) confirm this structural difference across the exterior, interior, frequency and initial-state slices, certifying that the Hayward-induced behaviour reported in Figs. 2–5 is intrinsically tied to Fermi–Dirac statistics. This is in line with the same fermionic signature recently reported for the Reissner–Nordström geometry in Ref. [12].

VIII. LIMITATIONS AND DISCUSSION

Three aspects of the calculation deserve explicit discussion before drawing final conclusions: (i) the single-mode approximation that underpins (12); (ii) the role of the inner Cauchy horizon specific to regular black holes; (iii) the choice of the Boulware–Hartle–Hawking versus Unruh vacuum.

A. Single-mode approximation

The Bogoliubov transformation (12) is a single-mode identification of the Kruskal vacuum, in which a Kruskal

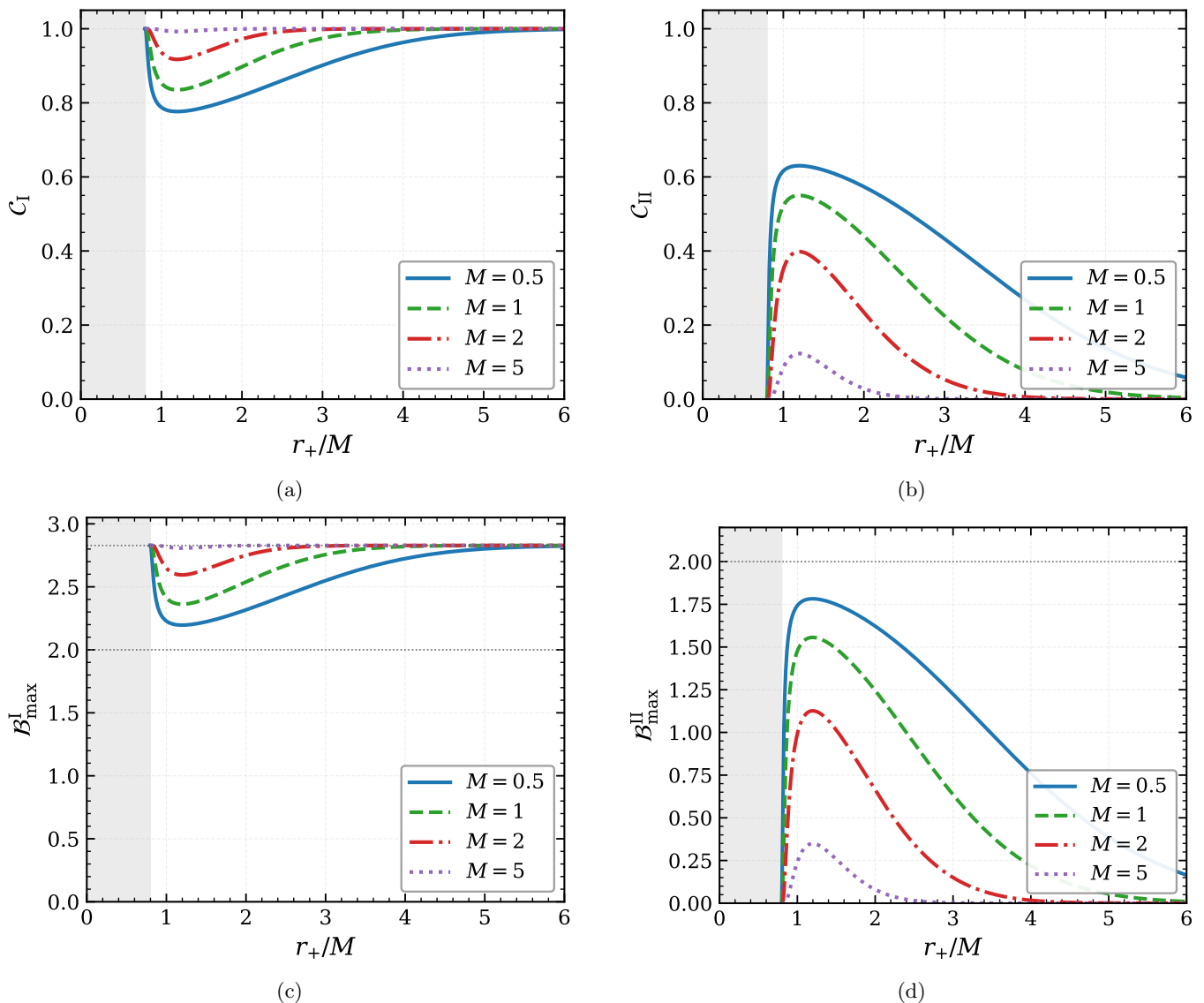


FIG. 3: Same quantities as in Fig. 2, plotted versus r_+/M for four values of the black-hole mass $M \in \{0.5, 1, 2, 5\}$ at fixed ratio $g/M = 0.5$, $\omega = 0.05$, $\alpha = \pi/4$. Heavier (colder) holes saturate the Tsirelson bound at smaller r_+/M .

annihilation operator is mapped to a linear combination of a single Schwarzschild–Hayward outgoing mode in region I and a single ingoing mode in region II. As emphasised in Refs. [25, 26], this approximation is strictly valid only when the wavefunction of the mode in question is peaked sharply in frequency that the smearing across modes induced by the Bogoliubov mixing can be neglected. Beyond the single-mode approximation, the Kruskal annihilation operator is mapped to an integral over Schwarzschild–Hayward modes weighted by the wavefunction of the selected mode, and the reduced density matrix ρ_{AB_I} has its coherences modified by mode-dependent factors that do not change the qualitative behaviour but slightly suppress the accessible correlations [25]. The Hayward dependence unveiled in the present work is robust against this correction, since it

enters the analysis only through the local Hawking temperature at r_+ , which is a mode-independent quantity. The quantitative single-mode correction can be incorporated as a multiplicative factor in the Bogoliubov coefficients, leaving Eqs. (23)–(24) and their Hayward dependence formally unchanged but renormalising their absolute values.

B. Inner Cauchy horizon

The Hayward metric possesses an inner Cauchy horizon $r_- < r_+$, the smaller positive root of Eq. (4). As recently emphasised in the regular-black-hole literature [18, 19], the Cauchy horizon is generically unstable under the mass-inflation mechanism, leading to large

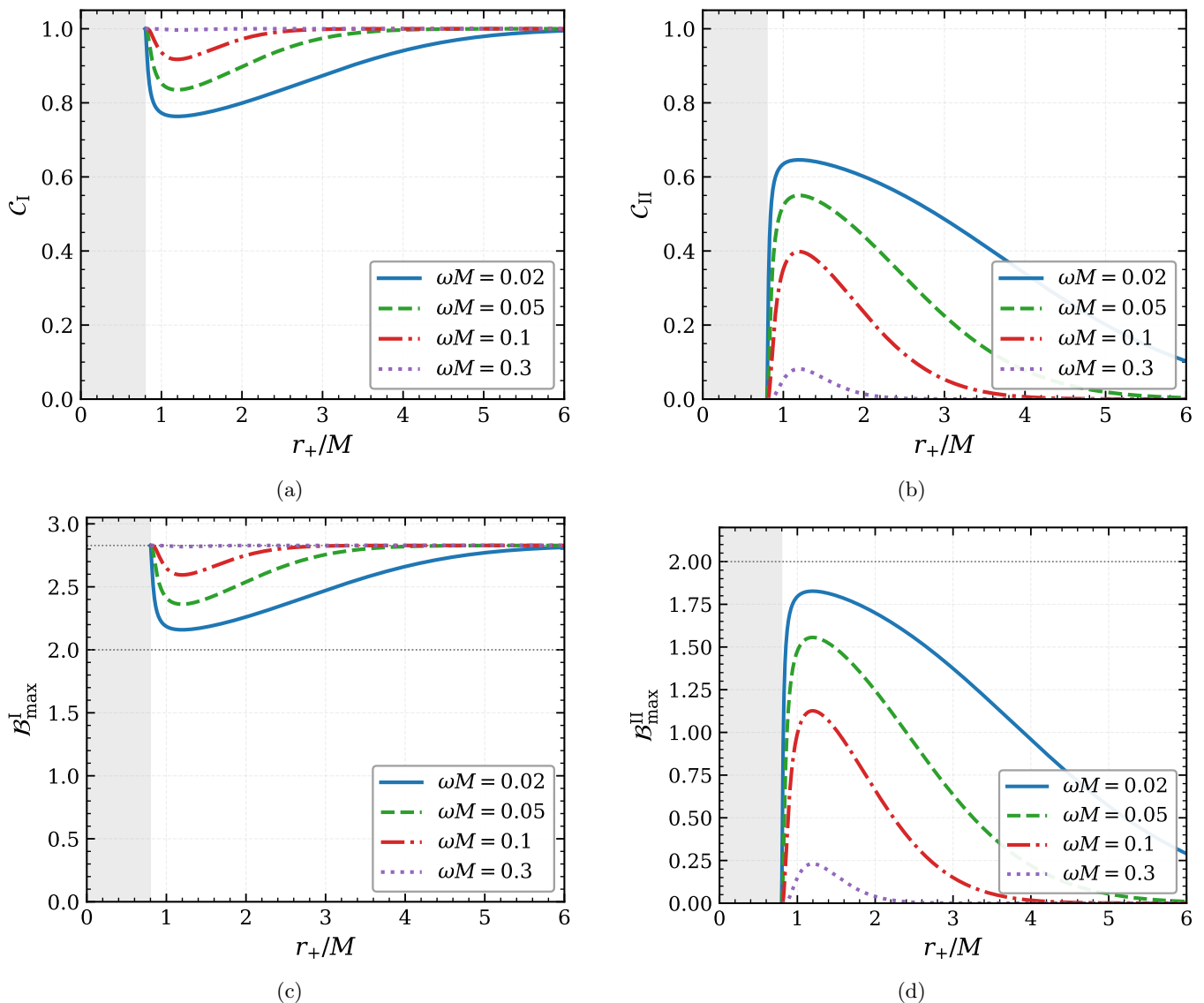


FIG. 4: Concurrences and CHSH parameters as functions of r_+/M for four mode frequencies $\omega M \in \{0.02, 0.05, 0.10, 0.30\}$, with $M = 1$, $g/M = 0.5$, $\alpha = \pi/4$. Higher frequencies suppress the Hawking factor $e^{-\omega/T_H}$ and accelerate the saturation to the Tsirelson bound.

curvature build-up in its vicinity even though the metric remains everywhere smooth. The quantum-information setup of the present work is not directly affected by this instability: the Hawking radiation responsible for decoherence is sourced by the surface gravity at r_+ , not r_- , and the static observer Bob is located outside the event horizon. However, the phenomenological status of the de Sitter core as a true vacuum is a delicate issue that ultimately constrains the validity of the Hayward semi-classical description at very small distances. Our analysis is robust against this caveat insofar as the only physical inputs are: (a) the surface gravity at r_+ , which is independent of the inner-horizon dynamics; and (b) the asymptotic Fock structure of the Dirac field, which is determined by the external geometry. Both inputs are

well-defined regardless of the fate of the Cauchy horizon.

C. Vacuum choice

The vacuum (12) corresponds to the Hartle–Hawking vacuum as seen by a static observer at fixed r outside the horizon [28–30]. A free-falling observer would see no Hawking quanta in the equivalence-principle sense; the entanglement degradation reported here pertains to the static observer specifically. This is the standard choice in the Dirac relativistic-quantum-information literature on Schwarzschild [3, 7, 9] and the one most relevant for terrestrial gedanken experiments (an observer with a rocket motor counteracting infall). The reader interested in the

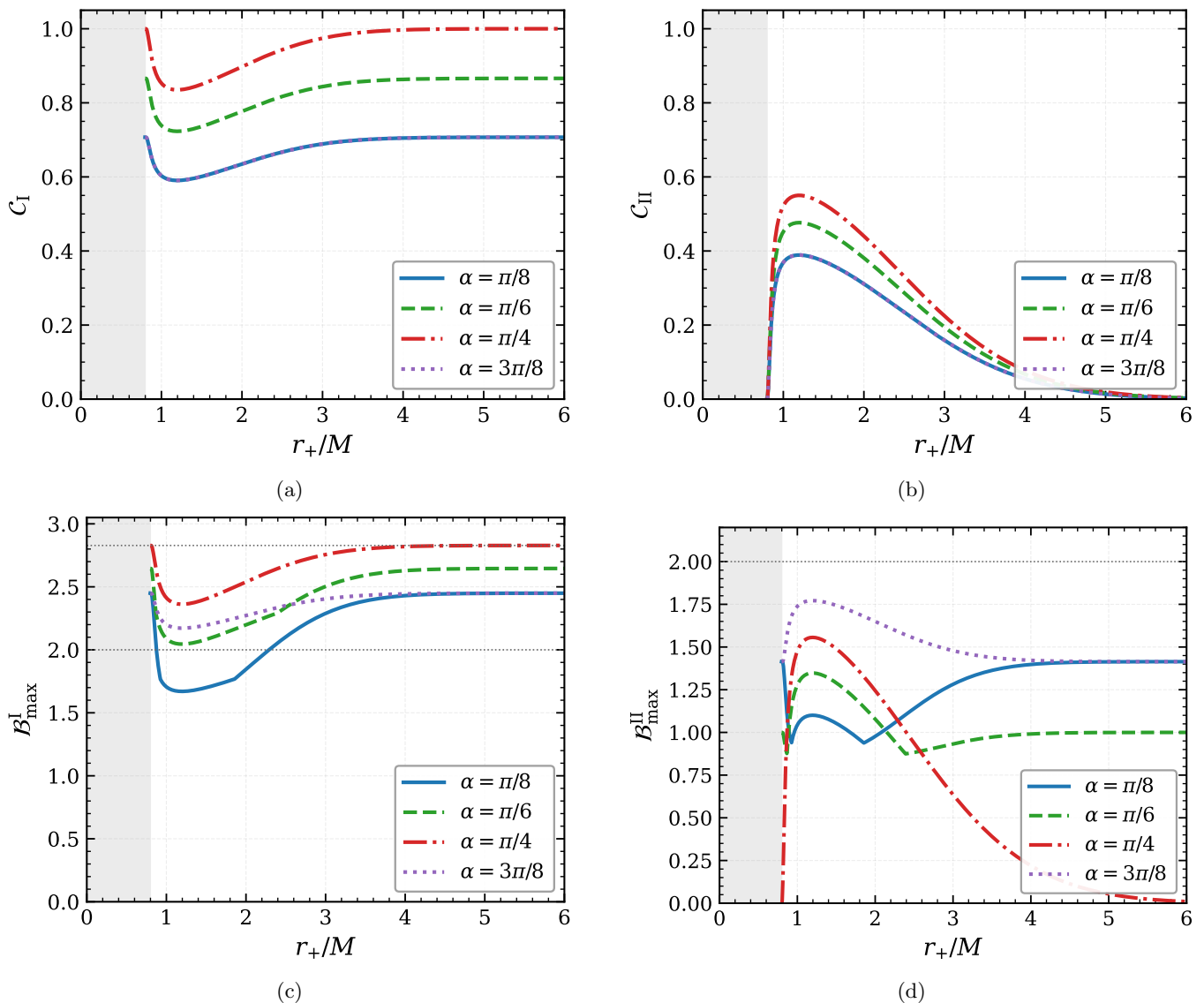


FIG. 5: Concurrences and CHSH parameters as functions of r_+/M for four mixing angles $\alpha \in \{\pi/8, \pi/6, \pi/4, 3\pi/8\}$, with $M = 1$, $g/M = 0.5$, $\omega = 0.05$. The Bell choice $\alpha = \pi/4$ maximises both quantities and is the only initial state for which \mathcal{B}_{\max}^I approaches the Tsirelson bound at large r_+ .

free-falling-observer perspective will find a complementary discussion in Refs. [11, 25, 26].

IX. CONCLUSION AND OUTLOOK

We have carried out a detailed study of the bipartite quantum correlations of a Dirac field in the background of a Hayward regular black hole, using the Wootters concurrence and the CHSH Bell parameter as two complementary indicators. Working in the standard Damour–Ruffini single-mode Bogoliubov framework, we derived the X-type reduced density matrices for both the accessible and the inaccessible sectors in closed form, and evaluated the two measures as functions of the four physical

control parameters: the regularity scale g , the black-hole mass M , the mode frequency ω , and the initial mixing angle α .

The following conclusions emerge from the analysis.

(i) The Hayward regularity parameter enters all quantities only through the Hawking temperature $T_H = T_H(g, M, r_+)$, and the qualitative response of the correlations is entirely controlled by the monotonic decrease of T_H with g .

(ii) Increasing g from 0 towards the extremal value $g_c \simeq 0.84 M$ enhances both the accessible concurrence \mathcal{C}_I and the accessible CHSH parameter \mathcal{B}_{\max}^I , and suppresses their inaccessible counterparts. At extremality ($T_H = 0$), the initial Bell entanglement is fully preserved in the exterior and no correlation crosses the horizon.

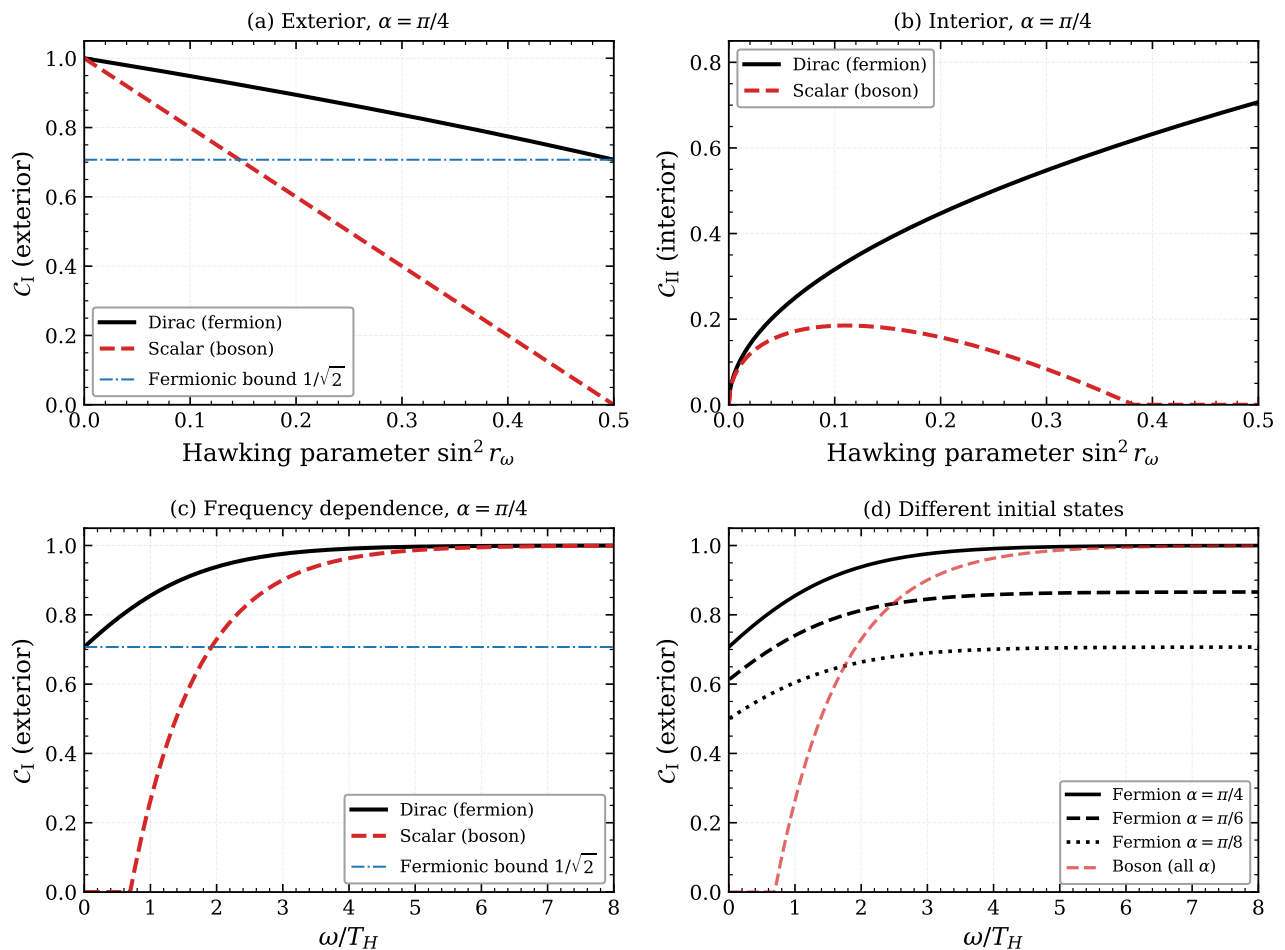


FIG. 6: Comparison of fermionic (Dirac, solid black) and bosonic (scalar, dashed red) concurrences. (a) Accessible concurrence \mathcal{C}_I as a function of the Hawking parameter $\sin^2 r_\omega = 1/(e^{\omega/T_H} + 1)$; the dash-dotted blue line indicates the fermionic lower bound $\sin(2\alpha)/\sqrt{2}$ of Eq. (26). (b) Inaccessible concurrence \mathcal{C}_{II} in the same regime.

(c) Frequency dependence ω/T_H at $\alpha = \pi/4$. (d) Multiple initial states $\alpha = \pi/4, \pi/6, \pi/8$. In all panels the fermionic concurrence remains above its structural Pauli bound, whereas the bosonic counterpart crosses below it and can vanish in the infinite-temperature limit. This panel certifies that the Hayward-induced behaviour reported in Figs. 2–5 is intrinsically tied to Fermi–Dirac statistics and cannot be reproduced by a scalar-field analysis.

(iii) The accessible CHSH parameter exceeds the classical limit 2 at every finite positive Hawking temperature when $\alpha = \pi/4$, with strength interpolating between the Tsirelson bound at $T_H \rightarrow 0$ and 2 at $T_H \rightarrow \infty$. The inaccessible CHSH parameter never violates the CHSH inequality, capped at 2 from above by the bound $\mathcal{B}_{\max}^{II} = 2\sqrt{2q} \leq 2$.

(iv) A direct comparison with the scalar (bosonic) analogue (Fig. 6) makes the genuinely fermionic character of our results explicit. The Pauli exclusion principle imposes the structural lower bound $\mathcal{C}_I \geq \sin(2\alpha)/\sqrt{2}$ and prevents the accessible correlations from ever vanishing, regardless of the values of g , ω , or r_+ in the physical Hayward range. The bosonic counterpart, in contrast, can undergo complete decoherence in the infinite-temperature limit. The Hayward-induced enhancement reported here is therefore not a generic feature of singu-

larity resolution but a specific consequence of fermionic statistics combined with the suppressed surface gravity of the regular geometry.

The overarching message is that the Hayward geometry, relative to its Schwarzschild reference, preserves Bell non-locality outside the event horizon more efficiently at fixed ADM mass. This translates the singularity-resolution programme into a quantitative quantum-information statement: the same parameter g that smoothes the central curvature also lowers the Hawking temperature and, with it, the gravitational decoherence experienced by external observers.

Several extensions naturally suggest themselves. First, the inclusion of realistic environmental decoherence channels [9, 10], in the spirit of the standard Kraus-operator formalism [42], would assess the robustness of the gravitational signatures in actual experimental settings. The

closed-form X-type structure of ϱ_{AB_I} and $\varrho_{AB_{II}}$ makes the addition of standard Kraus channels (amplitude damping, phase damping, depolarising) particularly tractable. Second, the generalisation to multipartite states (GHZ and W states across the horizon) and to other regular black holes (magnetically charged, Dymnikova, Frolov) is a natural follow-up. Third, the connection between the Hayward extension and the black-hole information paradox [2, 13] deserves further investigation: the explicit dependence of \mathcal{B}_{\max}^I on T_H may be exploited as a quantum-thermometric probe of the near-horizon geometry. Finally, the full calculation beyond the single-mode approximation, following the approach of [25, 26], would quantify the renormalisation of the absolute values of the bipartite measures without affecting the Hayward dependence. We hope that the closed-form analysis presented here will serve as a useful template for these generalisations.

ACKNOWLEDGMENTS

The authors thank the Laboratory of Theoretical Physics, Particles, Modeling and Energies, and the National Institute For Particle Physics and Applications (NIPPA, Oujda) for their hospitality and support. We are also grateful to the anonymous referee for detailed comments that improved the manuscript substantially, in particular regarding the discussion of the single-mode approximation.

DECLARATIONS

Funding: This research received no external funding.

Competing interests: The authors declare that they have no competing interests.

Data availability: The Python scripts used to generate the figures are included in the supplementary material and reproduce all results to machine precision.

-
- [1] Stephen W. Hawking. Particle creation by black holes. *Communications in Mathematical Physics*, 43(3):199–220, 1975.
- [2] Stephen W. Hawking. Breakdown of predictability in gravitational collapse. *Physical Review D*, 14(10):2460–2473, 1976.
- [3] Paul M. Alsing and G. J. Milburn. Teleportation with a uniformly accelerated partner. *Physical Review Letters*, 91(18):180404, 2003.
- [4] Ivette Fuentes-Schuller and Robert B. Mann. Alice falls into a black hole: Entanglement in noninertial frames. *Physical Review Letters*, 95(12):120404, 2005.
- [5] Gerardo Adesso, Ivette Fuentes-Schuller, and Marie Ericsson. Entanglement of dirac fields in noninertial frames. *Physical Review A*, 76(6):062112, 2007.
- [6] Jieci Wang, Qiyuan Pan, and Jiliang Jing. Projective measurements and generation of entangled Dirac particles in Schwarzschild spacetime. *Annals of Physics*, 325(6):1190–1197, 2010.
- [7] Shuai Xu, Xue-ke Song, Jia-dong Shi, and Liu Ye. Probing the quantum correlation and Bell non-locality for Dirac particles with Hawking effect in the background of Schwarzschild black hole. *Physics Letters B*, 733:1–5, 2014.
- [8] Shuai Xu, Xue-ke Song, Jia-dong Shi, and Liu Ye. How the Hawking effect affects multipartite entanglement of Dirac particles in the background of a Schwarzschild black hole. *Physical Review D*, 89(6):065022, 2014.
- [9] Juan He, Shuai Xu, Yang Yu, and Liu Ye. Property of various correlation measures of open Dirac system with Hawking effect in Schwarzschild space-time. *Physics Letters B*, 740:322–328, 2015.
- [10] Juan He, Shuai Xu, and Liu Ye. Measurement-induced nonlocality for Dirac particles in Garfinkle–Horowitz–Strominger dilation space-time. *Physics Letters B*, 756:278–282, 2016.
- [11] Jieci Wang and Jiliang Jing. Quantum entanglement of bosonic fields beyond the single-mode approximation in schwarzschild spacetime. *Physical Review A*, 82(3):032324, 2010.
- [12] Abdessamie Chhieb, Chaimae Banouni, Saliha Abdessamie, and Mohamed Ouchrif. Quantum entanglement in the Dirac field quantization around charged black holes. *Physics Letters B*, page 140629, 2026.
- [13] Sean A. Hayward. Formation and evaporation of nonsingular black holes. *Physical Review Letters*, 96(3):031103, 2006.
- [14] J. M. Bardeen. Non-singular general relativistic gravitational collapse. In *Proceedings of the International Conference GR5, Tbilisi, USSR*, page 174, 1968.
- [15] Irina Dymnikova. Vacuum nonsingular black hole. *General Relativity and Gravitation*, 24(3):235–242, 1992.
- [16] Eloy Ayón-Beato and Alberto García. Regular black hole in general relativity coupled to nonlinear electrodynamics. *Physical Review Letters*, 80(23):5056–5059, 1998.
- [17] Valeri P. Frolov. Information loss problem and a ‘black hole’ model with a closed apparent horizon. *Journal of High Energy Physics*, 2014(5):49, 2014.
- [18] Raul Carballo-Rubio, Francesco Di Filippo, Stefano Liberati, and Matt Visser. Phenomenological aspects of black holes beyond general relativity. *Physical Review D*, 98(12):124009, 2018.
- [19] Raul Carballo-Rubio, Francesco Di Filippo, Stefano Liberati, Costantino Pacilio, and Matt Visser. Inner horizon instability and the unstable cores of regular black holes. *Journal of High Energy Physics*, 2022(05):132, 2022.
- [20] William K. Wootters. Entanglement of formation of an arbitrary state of two qubits. *Physical Review Letters*, 80(10):2245–2248, 1998.
- [21] John F. Clauser, Michael A. Horne, Abner Shimony, and Richard A. Holt. Proposed experiment to test local hidden-variable theories. *Physical Review Letters*,

- 23(15):880–884, 1969.
- [22] R. Horodecki, P. Horodecki, and M. Horodecki. Violating Bell inequality by mixed spin- $\frac{1}{2}$ states: Necessary and sufficient condition. *Physics Letters A*, 200(5):340–344, 1995.
- [23] T. Damour and R. Ruffini. Black-hole evaporation in the Klein–Sauter–Heisenberg–Euler formalism. *Physical Review D*, 14(2):332–334, 1976.
- [24] Jiliang Jing. Hawking radiation of the Dirac field via an anomalous method. *Physical Review D*, 70(6):065004, 2004.
- [25] David Edward Bruschi, Jorma Louko, Eduardo Martín-Martínez, Andrzej Dragan, and Ivette Fuentes. Unruh effect in quantum information beyond the single-mode approximation. *Physical Review A*, 82(4):042332, 2010.
- [26] Eduardo Martín-Martínez and Ivette Fuentes. Entanglement in noninertial frames: Foundational issues. *Physical Review A*, 81(3):032320, 2010.
- [27] Dieter R. Brill and John A. Wheeler. Interaction of neutrinos and gravitational fields. *Reviews of Modern Physics*, 29(3):465–479, 1957.
- [28] William G. Unruh. Notes on black hole evaporation. *Physical Review D*, 14(4):870–892, 1976.
- [29] Werner Israel. Thermo-field dynamics of black holes. *Physics Letters A*, 57(2):107–110, 1976.
- [30] James B. Hartle and Stephen W. Hawking. Path-integral derivation of black-hole radiance. *Physical Review D*, 13(8):2188–2203, 1976.
- [31] N. D. Birrell and P. C. W. Davies. *Quantum Fields in Curved Space*. Cambridge University Press, 1984.
- [32] Paul M. Alsing, Ivette Fuentes-Schuller, Robert B. Mann, and Tracey E. Tessier. Entanglement of Dirac fields in non-inertial frames. *Physical Review A*, 74(3):032326, 2006.
- [33] Eduardo Martín-Martínez and Juan León. Fermionic entanglement that survives a black hole. *Physical Review A*, 80(4):042318, 2009.
- [34] Shin Takagi. *Vacuum noise and stress induced by uniform acceleration: Hawking–Unruh effect in Rindler manifold of arbitrary dimension*, volume 88. Progress of Theoretical Physics Supplement, 1986.
- [35] S. M. Hashemi Rafsanjani, M. Huber, C. J. Broadbent, and J. H. Eberly. Genuinely multipartite concurrence of N -qubit X -matrices. *Physical Review A*, 86(6):062303, 2012.
- [36] Q. Pan and J. Jing. Hawking radiation of Dirac particles via tunneling from the Reissner–Nordström black hole. *Modern Physics Letters A*, 23(1):25–34, 2008.
- [37] Eduardo Martín-Martínez and Ivette Fuentes. Entanglement in non-inertial frames: degradation and survival. *Physical Review A*, 83(5):052306, 2011.
- [38] B. S. Cirel’son. Quantum generalizations of Bell’s inequality. *Letters in Mathematical Physics*, 4(2):93–100, 1980.
- [39] Robert B. Mann and Timothy C. Ralph. Relativistic quantum information. *Classical and Quantum Gravity*, 29(22):220301, 2012.
- [40] Mehdi Ahmadi, David Edward Bruschi, Carlos Sabín, Gerardo Adesso, and Ivette Fuentes. Relativistic quantum metrology: Exploiting relativity to improve quantum measurement technologies. *Scientific Reports*, 4:4996, 2014.
- [41] Asher Peres and Daniel R. Terno. Quantum information and relativity theory. *Reviews of Modern Physics*, 76(1):93–123, 2004.
- [42] Karl Kraus. States, effects, and operations: Fundamental notions of quantum theory. *Lecture Notes in Physics*, 190, 1983.